Laboratory observation of hot bands of H_3^+

M. G. Bawendi, B. D. Rehfuss, and T. Oka
The Department of Chemistry and the Department of Astronomy and Astrophysics, The University of Chicago, Chicago, Illinois 60637

(Received 22 May 1990; accepted 3 July 1990)

The $(2\nu_2,l=2\leftarrow\nu_2)$, $(2\nu_2,l=0\leftarrow\nu_2)$, and $(\nu_1+\nu_2\leftarrow\nu_1)$ hot bands of H_3^+ were observed. The vibrationally hot ions were produced in a liquid nitrogen cooled 6 kHz ac discharge using gas mixtures of H_2 and He. The spectra were detected in direct absorption using a newly extended tunable difference frequency spectrometer using both $LiNbO_3$ and $LiIO_3$ crystals as nonlinear optical elements. The range of this spectrometer is now $\sim$5300–$\sim$1900 cm^{-1}. The positions of the rovibrational transitions compare extremely well with the theoretical predictions of Miller and Tennyson. A vibrational temperature study of the discharge indicates a significant population inversion between the ν_1 and ν_2 levels.

I. INTRODUCTION

Hydrogen is by far the most abundant element in the universe. The hydrogen molecule H_2 and various hydrides of carbon, nitrogen, and oxygen are the first molecules to form wherever matter begins to aggregate. This situation occurs, for instance, in dense interstellar clouds, star forming regions, and in the atmosphere of heavy planets where, unlike on earth, atmospheric escape of hydrogen has not occurred (e.g., Jupiter, Saturn, Uranus, and Neptune). A major participant in this dance to create molecules is the molecular ion H_3^+.[1-6]

Hydrogen molecules are ionized to H_2^+ by various astronomical processes such as cosmic ray bombardment, stellar photoionization, and collisional ionization by charged particles in magnetospheres. This is quickly followed by the formation of H_3^+ through the 1.7 eV exothermic reaction[7]

$$H_2^+ + H_2 \rightarrow H_3^+ + H \qquad (1)$$

which occurs with a large Langevin rate.[8,9] It is the subsequent reactions of H_3^+ with various other atoms and molecules present which leads to the synthesis of new ions and molecules. In addition to being a fundamental astrophysical species, H_3^+ is of great interest to molecular theorists. With just three protons and two electrons, H_3^+ is the simplest polyatomic system and as such has been an important testing ground for *ab initio* calculations.[10]

Since H_3^+ does not have stable electronic excited states,[11] structural and quantum mechanical information must be obtained from its rotational and vibrational spectra. With its D_{3h} symmetry and lack of permanent dipole moment, however, H_3^+ does not have pure rotational transitions except for very weak forbidden transitions.[12] Observation of its rotation–vibration spectrum in the infrared is then the easiest way to obtain spectral information. Its infrared spectrum is also the most effective means to use H_3^+ as an astronomical probe. It was in 1980 that the first 15 spectral lines belonging to the ν_2 fundamental band of H_3^+ were observed.[13] Since then a number of experimental studies have expanded the number of observed lines to over one hundred.[14,15] Theorists have been able to improve their potentials and calculations to the extent that they can now replicate experimental results for the ν_2 fundamental band to within $\sim$0.1 cm^{-1}.[16,17]

Miller and Tennyson[17] have recently predicted vibrational band origins and rotational terms for the $2\nu_2$, $\nu_1+\nu_2$, and ν_1 vibrational levels of H_3^+. Figure 1 shows their predictions and the infrared allowed transitions which fall in the region accessible by our difference frequency spectrometer. The value for the transition from the ground state to the ν_2 level was experimentally determined.[13] All three hot bands shown in Fig. 1 are at the lower edge of the range accessible with our $LiNbO_3$ based difference frequency system and are thus good candidates to test the $LiIO_3$ system which we have set up to scan from $\sim$5300 down to $\sim$1900 cm^{-1} and which is described in Sec. II.

Information on vibrationally excited states of H_3^+ is useful not only to *ab initio* theorists, but also to astrophysicists. Reaction (1) is known to yield H_3^+ ions in a distribution of vibrationally excited states and this has repercussions in the reactions of H_3^+ with other molecules. Kim *et al.*[18] have investigated the effects of this excess vibrational energy on the product distributions and rate constants for reactions of H_3^+ with a number of small molecules of astrophysical interest.

This paper reports the experimental observation of the three H_3^+ hot bands shown in Fig. 1. We have used our extended difference frequency spectrometer described previously[19] and in Sec. II to observe the $2\nu_2,l=2\leftarrow\nu_2$, $2\nu_2$, $l=0\leftarrow\nu_2$, and $\nu_1+\nu_2\leftarrow\nu_1$ transitions of H_3^+. The assignment was made through the use of combination differences and the predictions of Miller and Tennyson[17] which we found to be very accurate. The ions with excess vibrational energies were generated in liquid nitrogen cooled hydrogen/helium ac discharges. Velocity modulation detection was used to observe the transitions. We have also investigated the effects of He pressure and vibrational symmetry on deactivation of the excess vibrational energy.

The assignments and the accurately measured frequencies of the $2\nu_2(l=2)\leftarrow\nu_2$ band and the resulting absolute energy values for the vibration–rotation levels of the $2\nu_2(l=2)$ state reported in this paper have played a crucial role for the assignment of the 2 μm overtone emission band $2\nu_2(l=2)\rightarrow 0$ recently reported in the laboratory[20] and in

 0021-9606/90/216200-10$03.00

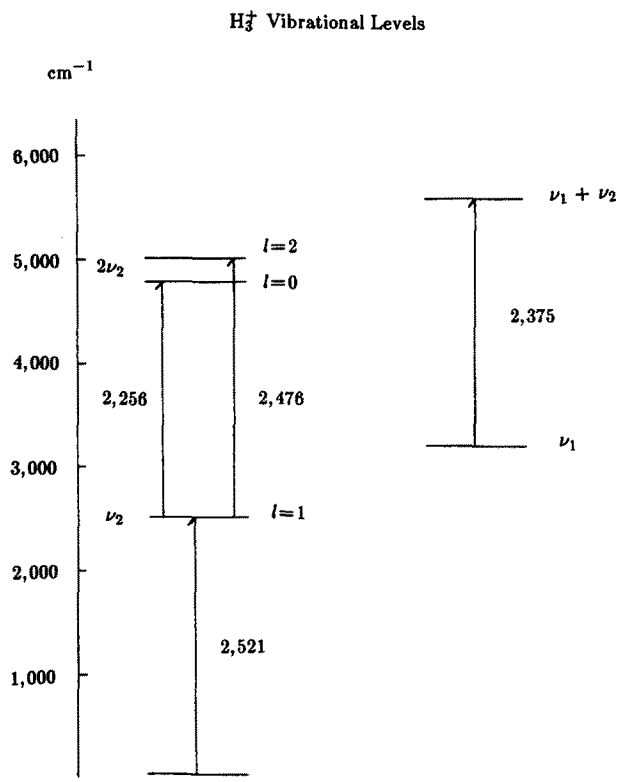

FIG. 1. Vibrational energy levels of H_3^+ as predicted by Miller and Tennyson (Ref. 17). The transitions shown are those which are infrared allowed and fall in the region accessible by our difference frequency spectrometer. The frequency for the transition from the ground state to the ν_2 level was experimentally determined (Ref. 13).

Jupiter.[21,22] It is also expected that the hot band spectrum of H_3^+ reported in this paper will be a useful astronomical probe to study planetary ionospheres and hot regions of molecular clouds that have been subjected to shocks.

II. EXPERIMENTAL DETAILS

The difference frequency spectrometer and the velocity modulation detection used to observe the hot bands of H_3^+ have been described in detail earlier.[19,23] We have now extended the reach of the spectrometer to scan from ~ 5300 to ~ 1900 cm^{-1} by using a paired set of angle tuned $LiIO_3$ crystals, roughly following the optical layout of Volkov *et al.*[24] The crystals used are cut at 22° with respect to the optic axis for phase matching at normal incidence at ~ 2300 cm^{-1}. Their dimensions are $30 \times 12 \times 6$ mm with a 1° wedge cut at one end of each crystal to prevent interference effects. The crystals were set in a mirror image arrangement so that the walkoff induced in the first crystal was reversed in the second. A combination of spherical and cylindrical lenses were used to focus the beam into the crystals so as to minimize the effects of walkoff. The infrared power from this $LiIO_3$ system was in the few to tens of μW with visible input powers of ~ 1 W in each color. To summarize, tunable infrared radiation was generated by mixing radiation from a fixed frequency argon ion laser with tunable radiation from a ring dye laser in either a temperature controlled $LiNbO_3$ crystal, or a paired set of angle tuned $LiIO_3$ crystals. The infrared was split into two beams of equal intensities. In the optical arrangement described previously,[19] one of the beams went through a discharge cell in a unidirectional multiple traversal White cell[25] arrangement before reaching a detector, while the second beam was directly sent to a detector for laser noise subtraction.[26] Noise subtraction was carried out by coupling the outputs of the detectors through two transformers wired out of phase of each other, and then sending the resulting signal to a phase sensitive detector (PSD) locked to the frequency of the ac discharge. In this arrangement, half of the precious power is diverted before reaching the sample cell and there is no cancellation of optical noise generated in the discharge tube.

We have improved the situation by using a bidirectional arrangement. Now both beams undergo unidirectional multiple traversals through the discharge cell, but *in opposite directions*. Noise subtraction is still carried out as before. Since one beam sees the ions Doppler shifted out of phase from the other beam, the signals due to ionic species add before reaching the PSD, while any laser noise or noise picked up from the discharge is subtracted. This optical arrangement results in twice as many passes going through the sample cell and thus in principle a doubling of the signal intensity. In practice, the signal to noise ratio is actually more than a factor of 2 better since the noise subtraction is more efficient with the two beams having the same path lengths and experiencing the same environment. The optimum number of traversals through the discharge results from a compromise between a longer absorption path length and an increase in noise due to the degradation of the infrared beam as its path length and the number of mirrors it hits increases. We have found that four traversals in each direction give the best signal to noise ratio.

A number of reference gases were used for frequency calibration depending on the spectral position. They were H_2CO,[27] N_2O,[28] HDO,[29] D_2O,[30] PH_3,[31] and CO.[28] Our frequency measurement accuracy was ~ 0.003 cm^{-1}.

In order to detect hot bands of H_3^+, we needed to generate H_3^+ in excited vibrational states, but we still wanted the ions to be rotationally fairly cold so that most of the spectral intensity would lie in the lower J states. Since reaction (1) is known to produce H_3^+ in a distribution of vibrationally excited states,[18] the goal was to keep making new ions through reaction (1) and to try to keep the ions vibrationally hot as long as possible.

A 6 kHz ac discharge and a multiple inlet–multiple outlet discharge cell were thus used in the hope that a fresh supply of vibrationally excited H_3^+ ions would be produced each time the discharge turned on. A large He buffer was chosen since collisions with He atoms should be a fairly inefficient mechanism for vibrational deactivation of the H_3^+ ions. The helium buffer also allowed us to use higher pressures than in pure hydrogen discharges. Higher pressures lead to a decrease in the electron drift velocities through collisions. The current and electron densities are related by

$$I = n_e A v_e e, \tag{2}$$

where I is the current, n_e is the electron density, A is the cross-sectional area of the discharge, v_e is the electron drift velocity, and e is the charge of an electron. According to Eq.

(2), for a fixed current and cross-sectional area, lower drift velocities thus imply a proportional increase in electron densities. Because of local charge neutrality in a discharge, this translates into higher ion densities and thus higher signal intensities.

Helium also has a higher ionization potential (24.6 eV) than H_2 (15.4 eV),[32] so that electron temperatures (and hopefully vibrational temperatures) are higher when He dominates in the discharge. Because of helium's low proton affinity (1.9 eV) compared to H_2 (4.5 eV),[32] the helium buffer is chemically fairly inert. We found that a large He buffer was crucial for observing H_3^+ hot bands.

Because rotation–translation energy transfer is much faster than vibration–translation energy transfer,[33] and the translational temperatures in discharges are known to be close to those of the cooling media, a liquid nitrogen cooled cell was chosen to achieve the low rotational temperatures desired. Liquid nitrogen cooling had the added benefit of further stabilizing the discharge.

In summary then, the discharge cell (the Black Widow) was a liquid nitrogen cooled multiple inlet–multiple outlet glass cell (see Ref. 19 for more details). A 6 kHz ac discharge with a current of ~130 mA was used to generate the ions and a H_2:He (1:10) mixture with a total pressure of ~7 Torr was found to produce vibrationally hot, yet rotationally cool H_3^+ ions.

The spectral regions from 2392 to 2854, 2882 to 2902, and 2932 to 2936 cm^{-1} were scanned continuously using the $LiNbO_3$ based difference frequency system. The gaps between the regions reflect areas where no hot band transitions were predicted either by Miller and Tennyson,[17] or by our preliminary results, or where atmospheric CO_2 has strong absorptions. The $LiIO_3$ system was used to scan the regions between 2086–2100, 2140–2172, 2228–2232, and 2240–2260 cm^{-1}. These areas were chosen because they contained the strongest P and Q branch lines.

Our sensitivity was decreased tremendously in going from $LiNbO_3$ at ~2900 cm^{-1} to $LiIO_3$ at ~2100 cm^{-1}. Mostly because of phase matching conditions and walk-off problems, the power output of the $LiIO_3$ system is ~40 times less than that of the $LiNbO_3$ system at the same frequency.[24,34,35] In principle, the infrared conversion efficiency is proportional to the square of the infrared frequency.[34,35] In practice, we found that at 2400 cm^{-1}, because of absorptions in the $LiNbO_3$ crystal and lower dye laser powers, the infrared power was actually an order of magnitude less than at ~2900 cm^{-1}. At 2100 cm^{-1}, using $LiIO_3$, the power was about two orders of magnitudes less than at 2900 cm^{-1} with $LiNbO_3$. The infrared power at ~2100 cm^{-1} was so low (a few μW), in fact, that our sensitivity was detector noise limited. If we assume that signal to noise ratios (S/N) are proportional to (power)$^{1/2}$ in regions where laser noise dominates, and proportional to the power where detector noise dominates, our S/N should then drop by a factor of ~3 and ~30 in going to 2400 and 2100 cm^{-1}, respectively, from 2900 cm^{-1}.

The average S/N observed for the R branch lines of the $2\nu_2, l = 2 \leftarrow \nu_2$ hot band was ~10 to 20, with the strongest lines ~100 to 200. Figure 2 shows one of the strongest R

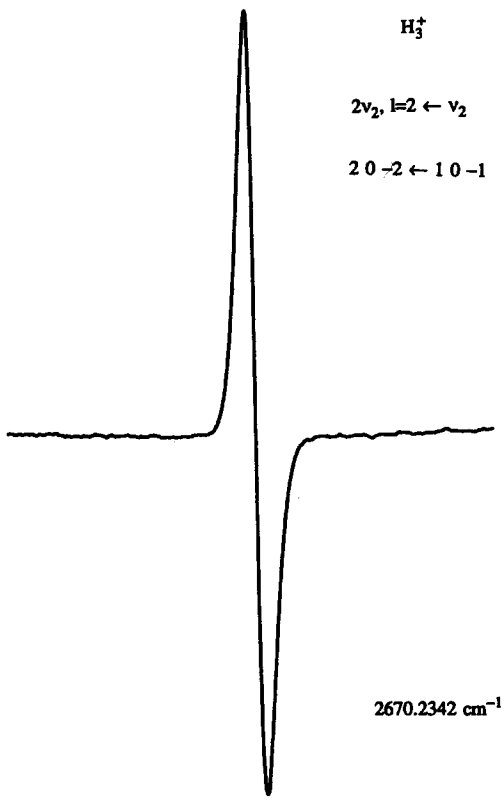

FIG. 2. An example of one of the strongest transitions (2 0 − 2 ← 1 0 − 1) in the spectrum of the $2\nu_2, l = 2 \leftarrow \nu_2$ band of H_3^+.

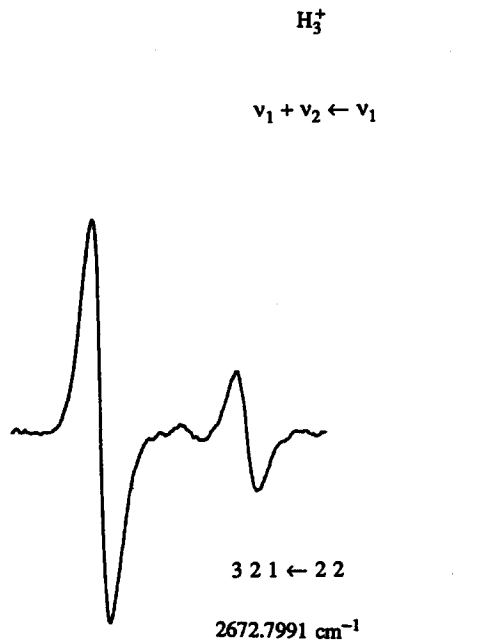

FIG. 3. An example of two transitions (4 3 − 1 ← 3 3 and 3 2 1 ← 2 2) in the spectrum of the $\nu_1 + \nu_2 \leftarrow \nu_1$ band of H_3^+.

branch lines for this band. In the P branch region around 2200 cm^{-1} where intensities are lower, we thus had no hope of seeing any but the strongest transitions and this turned out to be the case.

The $2\nu_2,l=0\leftarrow\nu_2$ hot band is predicted to be a factor of two less intense than the $2\nu_2,l=2\leftarrow\nu_2$ band due to the vibrational matrix element

$$\langle v,l\,|q_{\pm}\,|v-1,l\mp1\rangle=[(v\pm l)/2]^{1/2}. \quad (3)$$

Since the band origin of this hot band is predicted by Miller and Tennyson to be at $\sim$2256 cm^{-1},[17] we could not expect to see any but the strongest R branch lines.

The $\nu_1+\nu_2\leftarrow\nu_1$ hot band is also predicted to be a factor of 2 less intense than the $2\nu_2,l=2\leftarrow\nu_2$ band according to Eq. (3) if the number of molecules in the lower states of the transitions are assumed to be the same. However, the vibrational temperature of the symmetric ν_1 mode is expected to be higher than that of the antisymmetric ν_2 mode and thus the increase in population in the ν_1 mode could overcome the inherent lower intensity of the band. We were able to observe and assign a number of transitions in the $\nu_1+\nu_2\leftarrow\nu_1$ band, examples of which are shown in Fig. 3, and this allowed us to carry out vibrational temperature experiments to examine the effect of symmetry and He pressure on vibrational relaxation.

III. RESULTS

Two hundred and fifty four new transitions were observed in our hydrogen/helium discharge. It is very likely that almost all of them belong to H_3^+. Velocity modulation is very efficient in suppressing signals from neutral absorptions and the line shape gives a crude estimate of the mass of the absorbing species. Known HeH^+ transitions were found to be very weak due to our relatively large hydrogen pressure of $\sim$600 mTorr and the reaction

$$HeH^+ + H_2 \rightarrow He + H_3^+ \quad (4)$$

which has a rate constant of $k=1.8\times10^{-9}$ cm^3s^{-1}.[32]

On the basis of observed ground state combination differences and ν_2 energy levels given by Majewski *et al.*,[15] we were able to definitely assign 14 of the new absorptions to the ν_2 fundamental band of H_3^+. These transitions are given in Table I.

We found a number of transitions between 2400 and 2600 cm^{-1} which were within $\sim$0.7 cm^{-1} of the predictions of Miller and Tennyson[17] for the Q branch of the $2\nu_2,l=2\leftarrow\nu_2$ band. Since the ν_2 energy levels have been very thoroughly determined experimentally within each $G=|k-l|$ stack, temporary assignments of the lines gave us experimental energy levels for the $2\nu_2,l=2$ vibrational state. To confirm our assignments, it was then only necessary to observe a second transition going to the same upper state. We were eventually able to definitely assign 67 lines to the $2\nu_2,l=2$ band, corresponding to 38 upper state energy levels. Table II gives the observed and assigned transitions of the $2\nu_2,l=2\leftarrow\nu_2$ band, while Table III provides experimental energy levels for the $2\nu_2,l=2$ state. As discussed in the previous section, the $2\nu_2,l=0\leftarrow\nu_2$ band was much harder to observe than the $l=2$ band. We were eventually able to assign 14 lines to this band as given in Table IV which yielded 13 upper state energy levels. Table V provides the experimental energy levels for the $2\nu_2,l=0$ state.

TABLE I. New observed transitions in the $\nu_2\leftarrow0$ fundamental band of H_3^+ (in cm^{-1}).[a]

J_g	G_g	U_g	←	J_l	K_l	ν_{obs}
5	4	−1		5	4	2467.5529
5	0	−1		5	0	2471.9229
3	1	1		3	1	2568.7032
7	7	1		7	7	2574.8943
9	9	1		9	9	2575.1115
8	8	1		8	8	2575.3115
4	2	1		4	2	2582.9088
4	1	1		4	1	2589.5406
7	6	1		7	6	2591.3226
8	7	1		8	7	2594.4767
5	2	1		5	2	2605.9213
7	5	1		7	5	2613.5400
6	3	1		6	3	2624.9671
5	1	−1		4	1	2889.0524

[a] 5 0–1 ← 5 0 was misassigned in Ref. 15.

Assignment of lines to the $\nu_1+\nu_2\leftarrow\nu_1$ band was not as straightforward. Miller and Tennyson's predictions[17] turned out to be very accurate for the $2\nu_2,l=2\leftarrow\nu_2$ band, with on the average an error of $\sim$0.6 cm^{-1}, but part of the reason for this level of accuracy could be attributed to the experimental data already available on the ν_2 fundamental band. It was not clear to us that their predictions for the $\nu_1+\nu_2\leftarrow\nu_1$ transitions, with no experimental information available on either the ground state or the upper state, would be as accurate as for the $2\nu_2,l=2\leftarrow\nu_2$ band. In addition, confirmation of assignments for $\nu_1+\nu_2\leftarrow\nu_1$ transitions based on combination differences here need four transitions since no experimental data is available on either the upper state or the lower state. And at least one of these transitions needs to be in the P branch at $\sim$2100 cm^{-1}, where our sensitivity, as discussed in Sec. II, is very poor.

We observed a number of lines which were reasonably close to the predictions of Miller and Tennyson[17] for the $\nu_1+\nu_2\leftarrow\nu_1$ band. In most cases, however, too many possible experimental lines were close to the theoretical predictions to make an assignment. It was not until we observed the four lines in Table VI that form proper combination differences that we were confident that we had observed the $\nu_1+\nu_2\leftarrow\nu_1$ band of H_3^+. We were eventually able to assign 21 lines to the $\nu_1+\nu_2\leftarrow\nu_1$ band, mostly based on the predictions of Miller and Tennyson[17] and intensity considerations. These lines are presented in Table VI. We found the agreement with the theoretical predictions to be extremely good here also.

Since the intensities of the lines due to the $\nu_1+\nu_2\leftarrow\nu_1$ band were very reasonable, as shown in Fig. 3, some of the lines which remain unassigned are most certainly part of the $\nu_1+\nu_2\leftarrow\nu_1$ band. In fact, many of these unassigned lines lie close to theoretical predictions for this band. There are, however, too many experimental choices for each theoretical prediction to make a definite assignment. Most of the remaining 138 lines (listed in Table VII) are very weak and are

TABLE II. Observed and assigned transitions in the $2\nu_2, l = 2 \leftarrow \nu_2$ band of H_3^+ (in cm^{-1})[a].

J_g	G_g	U_g	←	J_l	G_l	U_l	ν_{obs}	ν_{calc}
5	6	2		6	6	1	2089.7638	2089.7
4	6	2		5	6	1	2168.3493	2168.3
3	5	2		4	5	1	2241.3466	2241.2
3	1	−2		3	1	1	2422.9831	2422.0
4	1	−2		4	1	1	2423.6751	2422.7
4	0	−2		4	0	1	2449.8004	2449.0
0	2	2		1	2	1	2449.8849	2449.4
4	2	−2		4	2	−1	2456.2727	2455.2
2	0	−2		2	0	1	2474.0543	2473.3
3	1	−2		3	1	−1	2483.5530	2482.7
4	1	2		4	1	1	2508.7571	2508.1
3	1	2		3	1	1	2510.2912	2509.6
2	1	2		2	1	1	2514.6191	2514.0
1	1	2		1	1	1	2515.7548	2515.1
4	1	−2		4	1	−1	2520.6767	2519.9
5	2	2		5	2	1	2534.9223	2534.4
4	2	2		4	2	1	2536.9314	2536.4
1	2	2		1	2	1	2539.4509	2539.0
5	3	2		5	3	1	2539.7444	2539.1
3	2	2		3	2	1	2541.2928	2540.8
3	0	2		3	0	−1	2541.4326	2540.8
2	2	2		2	2	1	2542.4670	2541.9
3	3	2		3	3	1	2554.2758	2553.8
2	3	2		2	3	1	2566.9039	2566.5
3	1	2		3	1	−1	2570.8584	2570.3
4	3	2		4	3	1	2577.6294	2577.3
5	4	2		5	4	1	2579.6715	2579.2
3	4	2		3	4	1	2579.7483	2579.4
4	4	2		4	4	1	2583.1554	2582.8
6	5	2		6	5	1	2590.3147	2589.7
4	5	2		4	5	1	2596.5199	2596.2
5	5	2		5	5	1	2599.2684	2598.9
3	2	2		3	2	−1	2602.3666	2602.0
1	1	2		0	1	1	2603.8831	2603.2
4	1	2		4	1	−1	2605.7634	2605.3
7	6	2		7	6	1	2606.1544	
5	6	2		5	6	1	2611.8378	2611.6
6	6	2		6	6	1	2615.0683	2614.8
6	7	2		6	7	1	2626.2198	2626.0
4	2	2		4	2	−1	2628.0974	2627.7
7	7	2		7	7	1	2628.1186	2627.8
7	8	2		7	8	1	2639.8058	2639.6
5	0	2		5	0	−1	2648.6924	2648.3
8	9	2		8	9	1	2653.0951	2652.9
5	3	2		5	3	−1	2660.3728	2660.0
4	3	2		4	3	−1	2665.7293	2665.6
2	0	−2		1	0	−1	2670.2342	2669.4
2	1	2		1	1	1	2695.4196	2694.7
3	1	−2		2	1	1	2696.1102	2695.0
2	2	2		1	2	1	2718.2616	2717.7
4	2	−2		3	2	1	2724.0581	2722.7
3	1	−2		2	1	−1	2730.8869	2729.9
5	3	−2		4	3	1	2737.8510	2736.3
6	4	−2		5	4	1	2740.5680	2739.3
3	0	2		2	0	1	2754.5347	2753.7
4	1	−2		3	1	1	2783.3247	2782.2
3	1	2		2	1	1	2783.4170	2782.7
4	2	−2		3	2	−1	2785.1212	2783.9
3	2	2		2	2	1	2809.7667	2809.2
3	3	2		2	3	1	2816.8426	2816.2
5	2	−2		4	2	1	2818.0717	2816.7
3	1	2		2	1	−1	2818.1960	2817.5
5	3	−2		4	3	−1	2825.9556	2824.6
6	4	−2		5	4	−1	2854.1911	2853.1
4	1	2		3	1	1	2868.4062	2867.7
4	0	−2		3	0	−1	2870.8895	2870.1
4	2	2		3	2	1	2895.8735	2895.2
4	4	2		3	4	1	2932.9879	2932.5
4	3	2		3	3	1	2934.1551	2933.8
5	0	−2		4	0	−1	2944.828	2944.0

[a] Calculated frequencies are from Miller and Tennyson (Ref. 17).

TABLE III. "Observed" energy levels for the $2\nu_2,l=2$ state of H_3^+ (in cm^{-1}).[a]

J	G	$U=-2$	$U=+2$
2	0	5286.918	
3	0		5567.393
4	0	5896.843	
5	0		6391.879
1	1		5125.298
2	1		5304.964
3	1	5486.454	5573.761
4	1	5846.794	5931.876
0	2		4998.056
1	2		5087.622
2	2		5266.433
3	2		5533.733
4	2	5716.493	5888.314
5	2	6169.455	6327.945
2	3		5181.186
3	3		5431.124
4	3		5811.004
5	3		6213.702
3	4		5299.241
4	4		5652.481
5	4		6089.830
6	4	6250.724	
3	5		5105.289
4	5		5460.462
5	5		5899.400
6	5		6415.749
4	6		5215.734
5	6		5659.222
6	6		6184.526
7	6		6784.060

[a] This table assumes the following experimentally determined ground state energy levels (Ref. 39): $F_0(1,0)=86.963$; $F_0(1,1)=64.125$; $F_0(2,2)=169.302$; $F_0(3,3)=315.352$; $F_0(4,4)=502.042$; $F_0(5,5)=729.020$; $F_0(6,6)=995.875$; and observed $\nu_2\leftarrow 0$ transitions (Refs. 14 and 15).

probably due to either unassigned high J transitions of the ν_2 fundamental band of H_3^+, $\Delta|k-l|=6$ forbidden transitions of the ν_2 band, high J transitions of the $2\nu_2,l=2\leftarrow\nu_2$ and $\nu_1+\nu_2\leftarrow\nu_1$ bands, or higher hot bands.

A digression on notation is in order here. The rotation–vibration effective Hamiltonian for H_3^+ has an abnormally large l-resonance term which mixes the states $|k+1,l+1\rangle$ and $|k-1,l-1\rangle$ through the off-diagonal element

$$\tilde{H}_q = q_{\text{eff}}(q^2_+ J^2_+ + q^2_- J^2_-)/4, \tag{5}$$

where $q_{+(-)}$ and $J_{+(-)}$ are raising (lowering) operators for the vibrational levels and rotational levels, respectively. The usual quantum numbers k and l are thus not good quantum numbers any more and must be replaced by the good quantum number $G=|k-l|$. Watson[36] has introduced the U notation to label the two states with the same G quantum number which result from diagonalizing the 2×2 matrices caused by Eq. (5). In his notation for the ν_2 band, $U=-1$ labels the states with the lower energy and $U=+1$ labels the state with the higher energy. His notation has been generalized by taking $|U|=|l|$ for the $2\nu_2,l=2$ levels, so that $U=-2$ labels the states with the lower energy and $U=+2$ labels those with the higher energy. This notation is reflected in the assignments in Tables I–VI.

Because of the large perturbations in the $2\nu_2,l=2$ rotational levels due to their mixing with the rotational levels of the $2\nu_2,l=0$ state, a fit containing experimental information on only the $2\nu_2,l=2$ levels is necessarily incomplete and we clearly do not have enough $2\nu_2,l=0$ lines to give information about that level. In addition, because H_3^+ is such a light molecule with a shallow electronic potential, centrifugal distortion effects are very large. A reasonable fit of the data to standard effective Hamiltonians requires almost as many parameters as experimental data points. Results of the fits are thus not very useful in predicting new transitions. Fits of the $2\nu_2$ rotational levels were thus not pursued and not enough experimental lines are thus far available to properly fit the

TABLE IV. Observed and assigned transitions in the $2\nu_2,l=0\leftarrow\nu_2$ band of H_3^+ (in cm^{-1}).[a]

J_g	K_g	←	J_l	G_l	U_l	ν_{obs}	ν_{calc}
2	2		1	2	1	2394.5563	2393.3
2	1		1	1	1	2413.9221	2412.7
3	3		2	3	1	2464.6524	2463.4
3	2		2	2	1	2486.8442	2485.5
3	1		2	1	1	2491.9760	2490.7
3	0		2	0	1	2492.7284	2491.4
4	4		3	4	1	2532.2527	2530.9
4	3		3	3	1	2557.4841	2556.1
5	3		4	3	1	2597.0576	2595.5
4	2		3	2	−1	2612.8420	2611.5
5	4		4	4	1	2621.5139	2620.1
6	6		5	6	1	2657.6519	2656.3
6	5		5	5	1	2683.7549	2682.3
5	3		4	3	−1	2685.1566	2683.7

[a] Calculated frequencies are from Miller and Tennyson (Ref. 17).

TABLE V. "Observed" energy levels for the $2\nu_2, l=0$ state of H_3^+ (in cm^{-1}).[a]

J	K	
3	0	5305.589
2	1	5023.465
3	1	5282.322
2	2	4942.727
3	2	5210.810
4	2	5544.213
3	3	5078.934
4	3	5434.330
5	3	5830.433
4	4	5251.746
5	4	5690.839
6	5	5983.887
6	6	5705.037

[a] This table assumes the following experimentally determined ground state energy levels (Ref. 39): $F_0(1,0)=86.963$; $F_0(1,1)=64.125$; $F_0(2,2)=169.302$; $F(3,3)=315.352$; $F_0(4,4)=502.042$; $F_0(5,5)=729.020$; $F_0(6,6)=995.875$; and observed $\nu_2 \leftarrow 0$ transitions (Refs. 14 and 15).

$\nu_1+\nu_2 \leftarrow \nu_1$ transitions. Probably the best strategy for this molecule is to provide the *ab initio* theorists with our experimentally determined energy levels so that they can further adjust with their potentials and accurately predict new rovibrational transitions. The exact shape of the potential is important not only for the spectroscopy of higher rovibrational states of H_3^+, but also for the reactions of H_3^+ which, as discussed in the introduction, are of astrophysical importance.

IV. TEMPERATURE STUDIES

Observation of the $2\nu_2, l=2 \leftarrow \nu_2$ and $\nu_1+\nu_2 \leftarrow \nu_1$ hot bands gives us the possibility of comparing the vibrational temperatures of the ν_2 and ν_1 modes in our discharges. The use of the term "temperature" is very loose here and is meant only to reflect the population ratios between the ground state and the ν_1 and ν_2 vibrational states. The concept of temperature assumes an equilibrium condition which is most certainly not present in our ac discharge and the reader is urged to keep this in mind. Nevertheless, the temperature (population ratios) measurements discussed in this section are still meaningful in understanding the relaxation processes in our hydrogen/helium plasmas.

In order to go from intensity ratios between rovibrational transitions to temperatures, either an experimental reference point or a theoretical estimate of the absorption intensities for the lines observed is needed. Since no experimental benchmark is yet available to measure temperatures of ionic species in plasmas, we need to rely on theoretical results.

Good theoretical intensities for transitions in the ν_2 band are available from its fit.[15] Since we do not know how much mixing there is between the different k levels of the $2\nu_2$ and $\nu_1+\nu_2$ states, however, it is important to choose transitions where, if possible, *no* mixing is allowed. The use of Höln–London factors should then give an accurate enough estimate of intensity ratios for these absorptions.[37]

An additional complication arises from our spectrometer. The infrared power generated and going through the

TABLE VI. Observed and assigned transitions in the $\nu_1+\nu_2 \leftarrow \nu_1$ band of H_3^+ (in cm^{-1}).[a]

J_g	G_g	U_g	←	J_l	K_l	ν_{obs}	ν_{calc}
3	3	1		4	3	2089.3052[b]	2089.0
3	4	1		4	4	2097.7451	2097.7
2	3	1		3	3	2168.6984	2168.4
1	2	1		2	2	2241.0773	2240.6
1	1	1		1	1	2399.7490	2399.2
2	2	1		2	2	2412.8589	2412.3
3	2	1		3	2	2420.2072	2419.6
3	3	1		3	3	2424.7965[b]	2424.4
4	3	1		4	3	2433.9009[b]	2433.8
4	4	1		4	4	2438.5087	2438.3
2	1	−1		1	1	2538.2526	2537.4
2	0	1		1	0	2572.2203	2571.5
3	2	−1		2	2	2606.2958	2605.4
3	1	−1		2	1	2613.9324	2613.1
3	1	1		2	1	2671.1417	2670.4
3	2	1		2	2	2672.7991	2672.1
4	3	−1		3	3	2672.9580[b]	2672.1
4	2	−1		3	2	2680.6312	2679.8
4	2	1		3	2	2767.6777	2766.9
4	3	1		3	3	2769.3931	2768.8
4	0	1		3	0	2770.9402	2770.1

[a] Calculated frequencies are from Miller and Tennyson (Ref. 17).
[b] These lines form proper combination differences which confirm their assignments.

TABLE VII. Unassigned lines in our discharge (most likely of H_3^+) (in cm^{-1}).

2395.5004	2573.0569	2653.8848	2735.5152	2824.7543
2402.6214	2577.4920	2660.6382		
2403.3498	2577.6937	2664.2129	2742.6968	2836.0277
2405.0312	2579.3896	2666.1424	2743.4181	2838.0412
2406.0287	2579.8283	2666.4995	2744.5863	2841.1479
2413.3139	2590.0708	2672.8624	2744.7191	2842.1913
2416.2885	2595.8802	2673.2289	2745.3069	2844.5211
2418.8991	2597.7020	2674.3441	2747.4572	2851.4334
2419.5577	2605.0631	2679.4872	2748.1057	2852.1555
2420.7279	2611.4706	2680.3304	2754.3191	2853.5984
2421.8883	2612.5381	2680.4849	2756.1422	2862.1507
2436.6526	2614.0222	2681.4999	2762.2496	2864.3691
2454.4174	2617.8093	2685.9416	2766.0318	2868.0400
2457.6134	2620.5885	2699.3344	2769.8633	2869.5354
2457.9117	2622.8936	2700.5728	2770.1959	2882.7947
2458.8504	2623.2738	2702.3213	2771.5862	2890.9930
2469.2354	2626.2887	2704.3821	2787.4003	2893.1030
2470.6052	2630.4918	2708.4319	2789.7360	2893.3693
2471.3844	2630.6026	2708.7781	2795.2134	2895.6001
2477.7971	2630.8139	2709.4051	2798.6197	2896.1605
2483.9766	2640.1721	2709.4791	2801.1079	2898.6139
2491.9055	2648.1046	2713.7888	2807.2482	2901.5159
2497.3493	2649.3151	2715.5589	2810.5967	2901.6529
2498.0795	2650.5606	2716.8434	2817.3493	2902.5229
2509.7258	2650.9544	2719.4371	2821.5178	2932.7106
2554.4745	2653.2904	2725.3415	2822.3566	2934.3551
2570.9867	2653.5591	2733.6386	2822.4478	
2572.3573	2653.6923	2734.5263	2822.7301	

sample cell is not very stable; even within a single 1 cm^{-1} scan, the power may fluctuate quite a bit. It was then important to find absorptions which were as close together as possible and at the very least within 0.9 cm^{-1} of each other. Each temperature measurement was taken three times to average over the infrared power fluctuations.

Rotational temperatures for the ground state were obtained using intensity ratios from the 5 3 — 1←4 3 (ν_2←0) and 5 4 — 1←4 4 (ν_2←0) transitions. Rotational temperatures for the ν_2 levels were obtained indirectly combining intensity ratios of the 2 3←2 3 1 ($2\nu_2, l=2\leftarrow\nu_2$) and 4 4 1←4 4 ($\nu_2$←0) absorptions with ratios of the 4 4 2←4 4 1 ($2\nu_2, l=2\leftarrow\nu_2$) and 4 2 1←4 2 ($\nu_2$←0) transitions. The rotational temperatures of the ground state and ν_2 vibrational level are shown with crosses and circles in Fig. 4 as a function of He pressure.

It is widely assumed that rotational and translational temperatures in discharges are roughly the same. Since we flow our gases through the liquid nitrogen cell, the translational temperatures of the incoming gases are between room temperature (298 K) and liquid nitrogen temperature (77 K). The discharge heats these gases up a bit and this is reflected in the ground state rotational temperatures which are in the range of 300 to 400 K. Helium has a higher ionization potential (24.6 eV) than H_2 (15.4 eV),[32] so that electron temperatures (and thus translational and rotational temperatures) are higher when He dominates in the discharge. The rotational temperature curve of the ground state as a function of He pressure in Fig. 4 thus follows the expected pattern.

The rotational temperature of the ν_2 state as shown in Fig. 4, on the other hand, starts fairly high at low He pressures and settles down to close to the rotational temperature of the ground state as the He pressure is increased. The explanation for this behavior is straightforward. Collisions with H_2 molecules efficiently deactivate excited vibrational states of H_3^+. According to Kim *et al.*,[18] the reaction

$$(H_3^+)^* + H_2 \rightarrow H_2^* + H_3^+ \qquad (6)$$

has a rate constant of $\sim 2.7\times 10^{-10}$ cm^3/s, where $(H_3^+)^*$

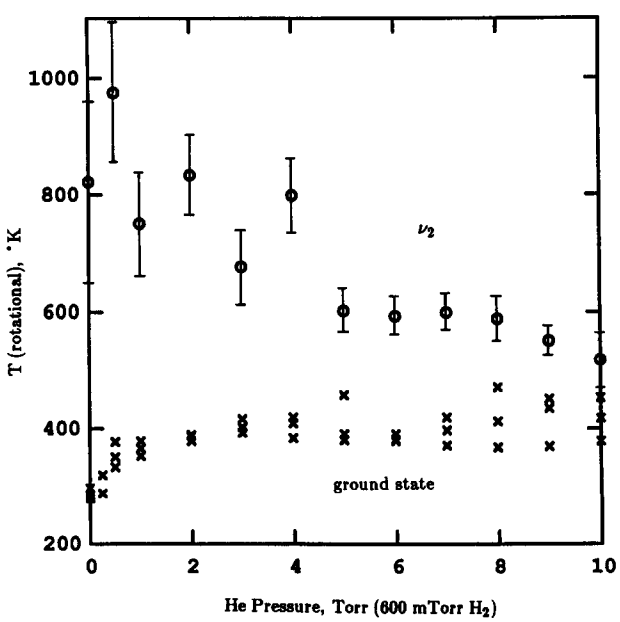

FIG. 4. Rotational temperature of H_3^+ as a function of He pressure for a fixed H_2 pressure of 600 mTorr. The rotational temperatures of the ground state are shown with (×), while those of the ν_2 state are denoted by (○).

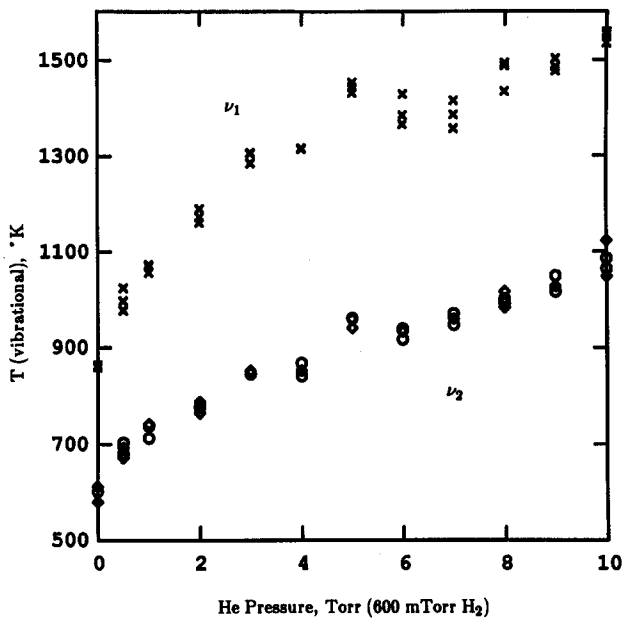

FIG. 5. Vibrational temperatures of H_3^+ as a function of He pressure for a fixed H_2 pressure of 600 mTorr. The vibrational temperatures of the ν_1 level are shown with (×), while those of the ν_2 state are denoted by (◇) using data from 2 3 2←2 3 1 and (○) using data from 4 4 2←4 4 1.

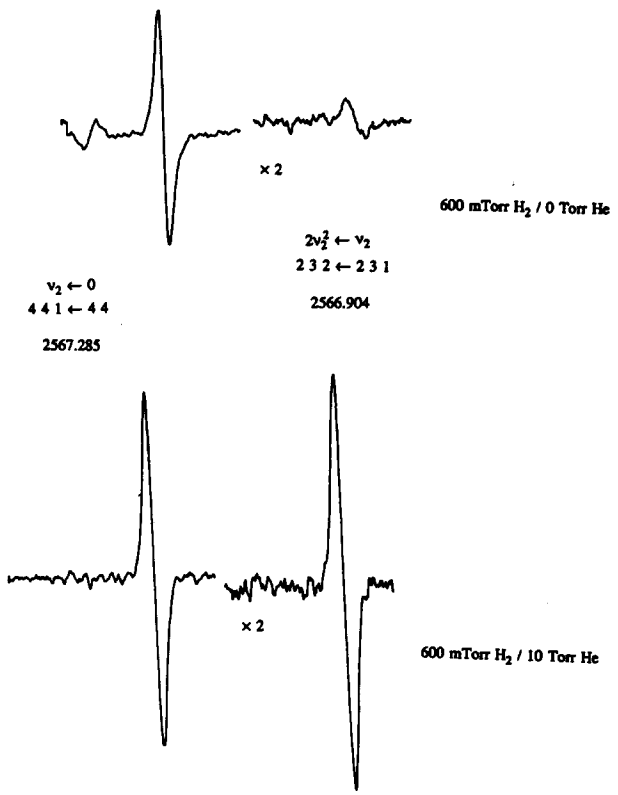

FIG. 6. An example of the increase in hot band signal when He dominates in the discharges. The top trace was taken with no He in the discharge cell, while the bottom trace was taken with 10 Torr He in the discharge cell. In both cases, the hot band was observed with a sensitivity setting of twice that for the fundamental.

indicates ions in a distribution of excited vibrational states. The mechanism for this deactivation can include either a proton hop from H_3^+ to H_2, a long-lived H_5^+ intermediate, or energy transfer to high rotational states of H_2. In any case, molecules in the ν_2 state are probably deactivated very fast when H_2 dominates in the discharge. When the H_3^+ ions are generated, the rotational level populations reflect formation mechanisms and are presumably non-Boltzmannian. If the ions are allowed to equilibrate with their environment as is the case for those in the ground state, rotational temperatures then mimic translational temperatures. However, for ions in the ν_2 state, vibrational deactivation through collisions with H_2 appears to be fast enough to prevent relaxation of the rotational populations, but when He dominates in the discharge and most collisions involve H_3^+-He pairs, the vibration–translation energy transfer is slow and the rotational temperature of the ν_2 state has time to equilibrate.

Vibrational temperatures of the ν_2 state were obtained from comparing intensity ratios of the 2 3 2←2 3 1 ($2\nu_2, l = 2 \leftarrow \nu_2$) and 4 4 1←4 4 ($\nu_2 \leftarrow 0$) transitions and also from the 4 4 2←4 4 1 ($2\nu_2, l = 2 \leftarrow \nu_2$) and 4 2 1←4 2 ($\nu_2 \leftarrow 0$) transitions. This gave two independent vibrational temperature determinations which are consistent with each other as shown with circles and diamonds in Fig. 5. Vibrational temperatures of the ν_1 state, shown with crosses in Fig. 5, were obtained indirectly by using intensity ratios from the 3 1 1←2 1 ($\nu_1 + \nu_2 \leftarrow \nu_1$) and 2 0 − 2←1 0 − 1 ($2\nu_2, l = 2 \leftarrow \nu_2$) transitions and using the vibrational and rotational temperatures determined from the ν_2 state.

The vibrational temperatures of both the ν_1 and ν_2 states increase with the pressure of He as is expected from the previous discussion on rotational temperatures. Figure 6 shows the dramatic increase in signal from the ν_2 level as the He pressure and thus the vibrational temperatures are increased. The striking feature in Fig. 5 is the significantly higher vibrational temperatures of the ν_1 state compared with the ν_2 state. It is this higher temperature which, as discussed in Sec. II, allowed us to observe the $\nu_1 + \nu_2 \leftarrow \nu_1$ transitions with reasonable signal to noise ratios. The higher temperature reflects a dependence on symmetry of the vibrational deactivation processes. The vibrational deactivation rate is in some way dependent on the dipole matrix element $\langle \nu_2 | \mu | 0 \rangle$ for the ν_2 state and $\langle \nu_1 | \mu | 0 \rangle$ or $\langle \nu_1 | \mu | \nu_2 \rangle$ for the ν_1 state. Since $\nu_2 \leftarrow 0$ is strongly allowed, while $\nu_1 \leftarrow 0$ is forbid-

TABLE VIII. Population ratios n_{ν_1}/n_{ν_2} and ensuing effective temperatures between the ν_1 and ν_2 states of H_3^+ as a function of He pressure and at a fixed H_2 pressure of 600 mTorr.

He(Torr)	n_{ν_1}/n_{ν_2}	T_{eff} (K)
0	1.15	−1135
0.5	1.00	−1364
1	0.99	−1384
2	1.11	−1185
3	1.12	−1172
4	1.05	−1274
5	0.94	−1497
6	0.94	−1497
7	0.80	−2011
8	0.85	−1781
9	0.77	−2189
10	0.75	−2331

den and the intensity of the $\nu_1 \leftarrow \nu_2$ band is very small according to Carney and Porter,[38] it is not surprising that the vibrational deactivation rate for the ν_1 state is slower than that for the ν_2 state and this is reflected in their temperatures in Fig. 5. The temperatures of the ν_1 and ν_2 states indicate that 4%–6% of the H_3^+ ions in our discharge are in the ν_1 state, while 5%–7% are in the ν_2 state.

It is possible to calculate population ratios between the ν_2 and ν_1 states and effective "temperatures" between those two states. This is summarized in Table VIII. Note that since ν_2 is degenerate, the population ratio between the two states at $T = \infty$ should be $n_{\nu_1}/n_{\nu_2} = 0.5$ in equilibrium. As can be seen in Table VIII, there is a significant population inversion between the ν_1 and ν_2 levels giving rise to negative effective temperatures. This population inversion in our ac discharge suggests the possibility of a H_3^+ molecular ion laser at ~ 660 cm^{-1}, a region of the spectrum in need of a laser.

ACKNOWLEDGMENTS

We would like to thank S. Miller and J. Tennyson for providing us with their calculation prior to publication and H. J. Kimble for a discussion leading to the bidirectional multiple path arrangement. This work was supported by NSF Grant No. PHY-87-07025 and Air Force contract No. F04611-86-K0069. M.G.B. gratefully acknowledges the support of AT&T through a PhD fellowship.

[1]E. Herbst and W. Klemperer, Astrophys. J. **185**, 505 (1973).
[2]W. D. Watson, Rev. Mod. Phys. **48**, 513 (1976).
[3]A. Dalgarno and J. H. Black, Rep. Prog. Phys. **39**, 573 (1976).
[4]H. Suzuki, Prog. Theor. Phys. **62**, 936 (1979).
[5]S. S. Prasad and W. T. Huntress, Jr., Astrophys. J. Suppl. Ser. **43**, 1 (1980).
[6]S. S. Prasad and W. T. Huntress, Jr., Astrophys. J. **239**, 151 (1980).
[7]T. R. Hogness and E. G. Lunn, Phys. Rev. **26**, 44 (1925).
[8]D. P. Stevenson and D. O. Schissler, J. Chem. Phys. **29**, 282 (1958).
[9]H. Eyring, J. O. Hirshfelder, and H. S. Taylor, J. Chem. Phys. **4**, 479 (1936).
[10]R. N. Porter, Ber. Bunsenges. Phys. Chem. **86**, 407 (1982).
[11]C. W. Bauschlicher, S. V. O'Neal, R. K. Preston, H. F. Shaefer, and C. F. Bender, J. Chem. Phys. **59**, 1286 (1973).
[12]F. S. Pan and T. Oka, Astrophys. J. **305**, 518 (1986).
[13]T. Oka, Phys. Rev. Lett. **45**, 531 (1980).
[14]J. K. G. Watson, S. C. Foster, A. R. W. McKeller, P. Bernath, T. Amano, F. S. Pan, M. W. Crofton, R. S. Altman, and T. Oka, Can. J. Phys. **62**, 1875 (1984).
[15]W. A. Majewski, M. D. Marshall, A. R. W. McKeller, J. W. C. Johns, and J. K. G. Watson, J. Mol. Spectrosc. **122**, 341 (1987).
[16]S. Miller and J. Tennyson, J. Mol. Spectrosc. **126**, 183 (1987).
[17]S. Miller and J. Tennyson, J. Mol. Spectrosc. **128**, 530 (1988); **136**, 223 (1989).
[18]J. K. Kim, L. P. Theard, and W. T. Huntress, Jr., Int. J. Mass Spectrom. Ion Phys. **15**, 223 (1974).
[19]M. W. Crofton, M. F. Jagod, B. D. Rehfuss, W. A. Kreiner, and T. Oka, J. Chem. Phys. **88**, 666 (1988).
[20]W. A. Majewski, P. A. Feldman, J. K. G. Watson, S. Miller, and J. Tennyson, Astrophys. J. **347**, L51 (1989).
[21]P. Drossart, J. P. Maillard, J. Caldwell, S. J. Kim, J. K. G. Watson, W. A. Majewski, J. Tennyson, S. Miller, S. K. Atreya, J. T. Clarke, J. H. Waite, Jr., and R. Wagener, Nature **340**, 539 (1989).
[22]L. Trafton, D. F. Lester, and K. L. Thompson, Astrophys. J. **343**, L73 (1989).
[23]C. S. Gudeman, M. H. Begemann, J. Pfaff, and R. J. Saykally, Phys. Rev. Lett. **50**, 727 (1983).
[24]S. Yu. Volkov, D. N. Kozlov, P. V. Nikles, A. M. Prokhorov, V. V. Smirnov, and S. M. Chuksin, Sov. J. Quantum Electron. **11**, 135 (1981).
[25]J. U. White, J. Opt. Soc. Am. **32**, 285 (1942).
[26]D. J. Nesbitt, H. Petek, C. S. Gudeman, C. B. Moore, and R. J. Saykally, J. Chem. Phys. **81**, 5281 (1984).
[27]A. S. Pine, M. I. T. Lincoln Laboratory Report No. NSF/ASRA/DAR-78-24562.
[28]G. Guelachvili and K. N. Rao, *Handbook of Infrared Standards* (Academic, Orlando, 1986).
[29]N. Papineau, C. Camy-Peyret, J.-M. Flaud, and G. Guelachvili, J. Mol. Spectrosc. **92**, 451 (1982).
[30]N. Papineau, J.-M. Flaud, C. Camy-Peyret, and G. Guelachvili, J. Mol. Spectrosc. **87**, 219 (1981).
[31]A. Baldacci, V. M. Devi, K. N. Rao, and G. Tarrago, J. Mol. Spectrosc. **81**, 179 (1980).
[32]W. T. Huntress, Jr., Astrophys. J. Suppl. Ser. **33**, 495 (1977).
[33]J. T. Yardley, *Introduction to Molecular Energy Transfer* (Academic, New York, 1980).
[34]Y. R. Shen, *The Principles of Nonlinear Optics* (Wiley-Interscience, New York, 1984).
[35]A. Yariv, *Quantum Electronics* (Wiley, New York, 1975).
[36]J. K. G. Watson, J. Mol. Spectrosc. **103**, 350 (1984).
[37]G. Herzberg, *Molecular Spectra and Molecular Structure. II. Infrared and Raman Spectra of Polyatomic Molecules* (Van Nostrand Reinhold, New York, 1945).
[38]G. D. Carney and R. N. Porter, J. Chem. Phys. **65**, 3547 (1976).
[39]L.-W. Xu, C. Gabrys, and T. Oka, J. Chem. Phys. **93**, 6210 (1990) (following paper).